Caco-2: Predicting drug permeability and relationship with COVID-19 infected Caco-2 cells

Clifford W Fong

Caco-2: Predicting drug permeability and relationship with COVID-19 infected Caco-2 cells

Clifford W. Fong
Eigenenergy, Adelaide, South Australia, Australia.
Email: cwfong@internode.on.net

Keywords: Caco-2, drug cellular permeability, passive transcellular and paracellular diffusion, active transport, COVID-2019 or SARS-CoV-2; ACE2 receptor binding, spike serine proteases, S-RBD, TMPRSS2, M^{pro}, IC_{50}, host cell membrane fusion or endocytosis, translatome and proteome proteomics, linear free energy relationships, HOMO-LUMO; quantum mechanics;

Abbreviations: Structure activity relationships SAR, $\Delta G_{desolv,CDS}$ free energy of water desolvation, $\Delta G_{lipo,CDS}$ lipophilicity free energy, cavity dispersion solvent structure of the first solvation shell CDS, Dipole moment DM, Molecular Volume Vol, HOMO highest occupied molecular orbital, LUMO lowest unoccupied molecular orbital, HOMO-LUMO energy gap, linear free energy relationships LFER, Molecular docking binding energy BE, Receptor binding domain of S protein of SARS-CoV-2 S-RBD, transmembrane serine 2 protease TMPRSS2, angiotensin-converting enzyme 2 ACE2, main protease of SARS-CoV-2, M^{pro}, Permeability across Caco-2 cells in apical to basolateral direction $P_{app(AB)}$, Permeability across Caco-2 cells in basolateral to apical direction $P_{app(BA)}$, Efflux Ratio ER

Abstract

Detailed studies of the permeability of a very wide range of drugs into Caco-2 cells shows that active transport, passive transcellular and passive paracellular transport can be separately identified using the LFER method involving $\Delta G_{desolv,CDS}$, $\Delta G_{lipo,CDS}$ (both octane and octanol), dipole moment, molecular volume, and HOMO-LUMO gap. Active transport is dependent on the HOMO-LUMO energy gap. Transcellular passive permeability shows dependency on the cell membrane lipophilicity as measured by $\Delta G_{lipo,CDS}$ in n-octanol and the free energy of water desolvation $\Delta G_{desolv,CDS}$. Paracellular passive permeability shows dependency on the molecular volume in water. There is evidence that different Caco-2 cell lines in various literature permeability studies can result in varying contributions of active and passive transport modes for a given range of drugs.

Inhibition of SARS-CoV-2 infected Caco-2 cells can be studied using the LFER method to separate Caco-2 cell entry processes involving ACE2, TMPRSS2 or S-RBD from intracellular inhibitory processes. The extensive study by Ellinger [25] likely involves the inhibition of Caco-2 cell entry processes involving ACE2, TMPRSS2 or S-RBD. It is known that Caco-2 cells were the only human cell type of 13 tested refractory cell lines that supported efficient SARS-CoV replication and expression of the SARS-CoV receptor, ACE2, [38] and Chu [39] found both human Calu-3 cells and Caco-2 cells were best suited for studying SARS-CoV-2 replication. Ellinger's data for Caco-2 cells is a valuable source for evaluating the efficacy of SARS-CoV-2 therapeutics.

The in vitro IC_{50} and docking binding energies of SARS-CoV-2 inhibition of M^{pro}, ACE2, S-RBD, TMPRSS2 show that the overwhelming conclusion is that the HOMO, or LUMO or the HOMO-LUMO energy gap is the principal determinant of inhibition of M^{pro}, S-RBD, ACE2 and TMPRSS2. The exception to this rule is the inhibitory binding to the human {ACE2-S-RBD} combined receptor which is likely to be a result of counterposing contributions from $inhibitor_{HOMO} \rightarrow receptor_{LUMO}$ or $receptor_{HOMO} \rightarrow inhibitor_{LUMO}$ dominated interactions for both S-protein and ACE2.

Introduction

Caco-2 is a cell line of human colorectal adenocarcinoma cells usually used as a cell culture monolayer. The Caco-2 monolayer is widely used as an in vitro model of the human small intestinal mucosa to predict the absorption of orally administered drugs. There is a well established correlation between the in vitro apparent permeability (P_{app}) across Caco-2 monolayers and the in vivo oral fraction of drugs absorbed. Caco-2 results can predict of the human absorption for drugs which display active uptake or efflux or passively pass through the cell membrane by transcellular or the paracellular route. Transport in both directions (apical to basolateral (AB) and basolateral to apical (BA) across the cell monolayer allows an efflux ratio to be determined which provides an indicator as to whether a compound undergoes active efflux. The Caco-2 cell monolayer has most of the known intestinal transporters in a pattern similar to that for the small intestine, and can give information on the mechanism of intestinal drug absorption and drug-drug interactions. In absence of transporter and enzyme involvement in the Caco-2 monolayer, transport in the A-B and B-A direction is symmetrical: $P_{app}(AB) = P_{app}(BA)$. The efflux ratio ER = $\{P_{app}(BA) / P_{app}(AB)\} > 2$ normally indicates significant involvement of apical efflux transporters, although the ER is dependent on passive permeability as well. ER values between 1-2 are less determinate. Figure 1 schematically describes the various transport mechanisms. [1]

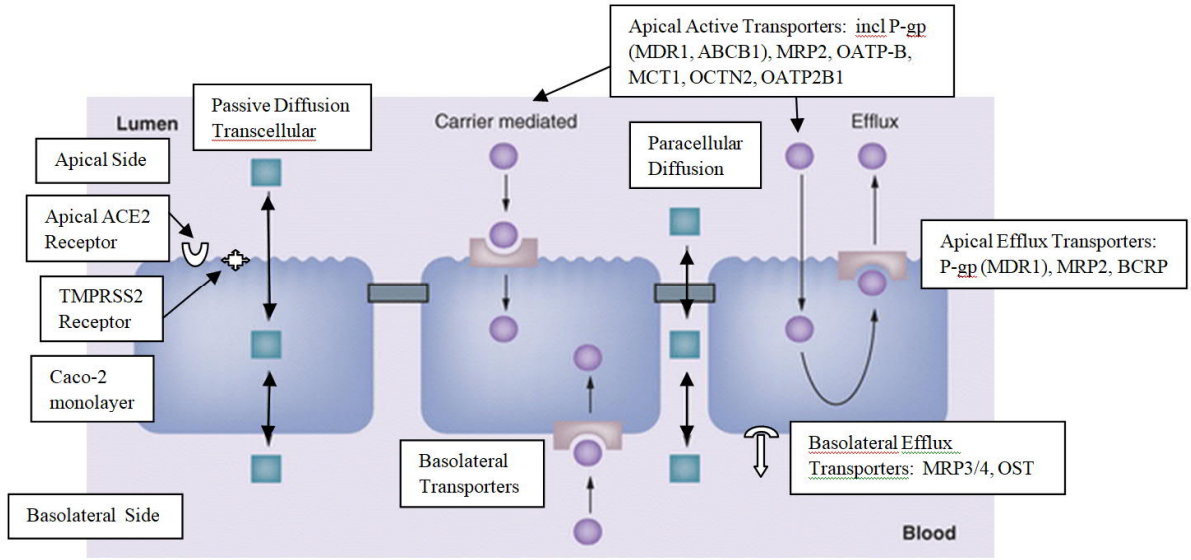

Figure 1. Transport mechanisms in Caco-2 cells and ACE2 and TMPRSS2 receptors

The overall permeation rate P_{app} for various drugs is the sum of all involved transport mechanisms: (a) passive diffusion across the monolayer, either directly through the cells (transcellular route) or through the water-filled pores in tight junctions interconnecting the cells (paracellular route), (b) facilitated diffusion or be actively transport against the concentration gradient either in the apical to basolateral (absorptive) or in the basolateral to apical (secretive) direction, (c) receptor mediated endocytosis or transcytosis, more common to peptides and larger molecules, and is of less importance for small molecules.

The characterization of passive permeability of drugs has usually been ascribed to their physicochemical properties in various QSAR studies. However, owing to the intrinsic heterogeneity of the parental cell line, and multiple clonal cell lines, culture-related conditions, as well as the different Caco-2 cell lines utilized in different laboratories, often makes it extremely difficult to compare various QSAR results in the literature. Inter-laboratory variations in P_{app} for various drugs are known to be large. One study showed that the standard deviation of published measurements for the same compound can reach almost 0.6 log units. [2-4]

Since efforts to identify accurate predictive structure activity relationships for the permeation of drugs across the Caco-2 cell membrane is known to be restricted by the large experimental errors that exist amongst different testing laboratories, [2,5] several studies have used the extensive experimental data of 52 widely disparate drugs from Yazdanian [6] to determine such predictive relationships. [7-9]

Lanevskij [3] analyzed by multistep non-linear multiple regression a literature database of 1366 Caco-2 permeability coefficients for 768 diverse drugs and drug-like compounds from varying experimental conditions (pH from 4.0 to 8.0) to develop a permeability model comprised of a minimal set of physicochemical descriptors: octanol-water log D, pKa, hydrogen bonding potential, and molecular size. Kim [10] found that the permeability coefficient for a series of model peptides in Caco-2 cells was dependent on octanol-water lipophilicity and hydrogen bonding potential. Milanetti [8] used the Yazdanian data set [6] and found that an analysis of the dynamic distribution of water molecules around 23 neutral drugs at pH 7.4 by molecular dynamics simulations, correlated well with the permeability measured using the Caco-2 cells. Ponce [7] used the Yazdanian data set [6] and found that the permeability coefficients in Caco-2 cells for 18 structurally diverse drugs (plus a training set of 33 drugs) were described by the quadratic indices of the molecular pseudograph's atom adjacency matrix as molecular descriptors. Santos-Filho [9] have used a membrane interaction QSAR approach based on the Yazdanian data set using 11 drugs (plus a training set of 30 drugs) quantum mechanically interacting with dimyristoylphosphatidylcholine (DMPC) molecule as the membrane monolayer surrogate model. It was concluded that Caco-2 cell permeation is governed by the spatial distribution of hydrogen bonding and nonpolar groups over the molecular shape of the DMPC monolayer.

In a wide and comprehensive review of 696 separate measurements from 15 collections of P_{app}(AB) of FDA approved drugs, O'Hagan [5] concluded that while inter-laboratory measurement variation varied by factors of 2-5, the P_{app} of marketed approved drugs is poorly

correlated with either simple biophysical properties, the extent of molecular similarity to endogenous metabolites (endogenites), or any specific substructural properties. The octanol:water partition coefficient, logP, shows negligible correlation with Caco-2 permeability. It was concluded that the data are best explained on the basis that most drugs enter (and exit) Caco-2 cells via a multiplicity of transporters of comparatively weak specificity. [5]

Epithelial tight junctions are known to contain size- and charge-selective pores that control the paracellular movement of charged and non-charged solutes. Van Itallie [11] showed that the paracellular (P_{app}) of a continuous series of non-charged polyethylene glycols (PEGs) across the monolayers of five different epithelial cell lines (including Caco-2), and porcine ileum, indicated two distinct pathways: (a) high-capacity small pores and (b) a size-independent pathway for larger solutes. All cell lines and ileum shared a pore aperture radius of 4 Å. Caco-2 cells have the largest numbers of pores as well as the greatest permeation through the size independent pathway of all epithelial cell lines. Camenisch [12] found that the permeability of a diverse range of structurally different drugs pass through Caco-2 cells by passive diffusion which can be predicted from the drugs' distribution coefficient in 1-octanol/water (log D(oct)) and its molecular weight (MW).

The lipophilicity of cell membranes is usually taken to be well represented by logD (to provide for charged species or logP for neutral species) in octanol at pH 7.4. Octanol is thought to be a suitable surrogate for phospholipid membranes as it mimics the hydrogen bonding ability of cell membranes. [12-15] We have previously used $\Delta G_{lipo,CDS}$ the free energy in n-octane as a measure of lipophilicity of drugs interacting with various targets, but for cell membrane targets, $\Delta G_{lipo,CDS}$ in octanol is a better measure. Octanol has been widely accepted as a membrane bilayer mimicking solvent, where the 2.18M equilibrium water concentration of n-octanol is consistent with the known water levels in cell membrane bilayer cores cause by some trans-bilayer water transport. [16] Octane has no hydrogen bonding capability. The lipophilicity of the cell membrane also has an effect on drugs trying to enter the membrane, so some degree of desolvation of water surrounding the drugs is required to facilitate entry into membrane. $\Delta G_{desolv,CDS}$ the free energy is a measure of water desolvation, the drug-water short-range interactions which includes contributions from hydrogen bonding capacity, as well as dispersion, exchange repulsion etc.

An important aspect that can have a significant effect on the Caco-2 passive permeability of various drugs is the potential ionization at physiological pH 7.4, particularly since many approved drugs are weak bases rather than acidic drugs. The pH partition theory suggests that while many drugs will be partly ionized at pH 7.4, it is mainly the neutral species that will be passively transported by 10^2 to 10^4 times as fast as their cationic or anionic counterparts. [17-19] Lee et al [20] similarly found that the neutral species of 14 acidic and basic drugs were preferentially transported across Caco-2 cells at pH 7.4 (and 6.5) rather than the ionized forms. Less is well known about active transport across Caco-2 cells. For example, digoxin, quinidine, verapamil, acebutolol, talinolol, Erythromycin, Ranitidine, cimetidine, Ritonavir, saquinavir, indinavir, nelfinavir, Taxol, doxorubicin, Zolmitriptan, Pimozide, reserpine, Chloroquine, domperidone, terfenadine, etc are actively intestinally transported by P-gp (MDR1, ABCB1) in Caco-2 cells, whereas the charged Estrone-3-Sulfate and Carnitine are transported by OATP2B1 and OCTN2 respectively.[1] Atenolol is known to be actively transported by OCT1 in MDCK

cells, whereas metoprolol is thought to be transported by facilitated diffusion. [21,22] Li [23] in their study of a new fast Caco-2 permeability test, identified that fexofenadine, cephalexin, digoxin, sulfasalazine, estradiol were known to be actively transported, and examined three transporters (PEPT1, OATP1A2, and P-gp) as well as their mediated influx or efflux and the increased gene expression of two excretive transporters (BCRP, MRP2).

A critical aspect of any quantitative structural activity study of the permeability of various drugs into Caco-2 cells is that a number of parallel mechanisms can occur: passive transcellular and paracellular diffusion, facilitated diffusion, and active transport processes. Comparing various data from different studies is confounded by possible variations in the actual Caco-2 cell line used, which may have inherent differences in membrane characteristics (affecting transcellular and paracellular diffusion) and active transporters. It is likely that multiple transport mechanisms may occur in transport studies of drugs in Caco-2 cell lines, for example both transcellular and paracellular diffusion for smaller neutral and less polarized drugs along with active transport for larger charged or more polarized drugs.

Fredlund [24] determined the apparent intrinsic permeability P_{app}(AB) across Caco-2 cell monolayers in the presence of an optimized cocktail of chemical inhibitors toward the three major efflux transporters ABCB1, ABCC2, and ABCG2. The intrinsic P_{app} values is thought to allow an estimate of passive permeability, which is independent of transporter expression levels and not limited by solubility or cell toxicity. Interestingly the drugs that showed passive permeability exhibited a similar (parallel) linear regression line for the intrinsic P_{app}(AB) versus P_{app}(AB) as did the drugs that were efflux inhibited.

Another topical use for Caco-2 cell assays is to identify repurposed therapeutic drugs that can be screened for efficacy against the SARS-CoV-2 virus. Ellinger [25] has screened a large number of approved drugs against SARS-CoV-2 infected Caco-2 cells, as well as against infected Vero-6, Calu-3 (human lung) or BHK-21 (hamster kidney fibroblast) cells. It is known that the ACE2 receptor is the entry port for the SARS-Cov-2 virus, and that mechanism is facilitated by the TMPRSS2 membrane protease. Both ACE2 and TMPRSS2 receptors are present on the apical surface of Caco-2 cells. Infected Caco-2 cells may be more sensitive than Vero-6 cells to the TMPRSS2 inhibitors, camostat and nefamostat, and may be better test bed for testing efficacy against the SARS-CoV-2 virus. Caco-2 cells have also been effectively tested against the SARS-CoV and MERS coronaviruses. Figure 2 describes how these receptors are present in Caco-2 cells.

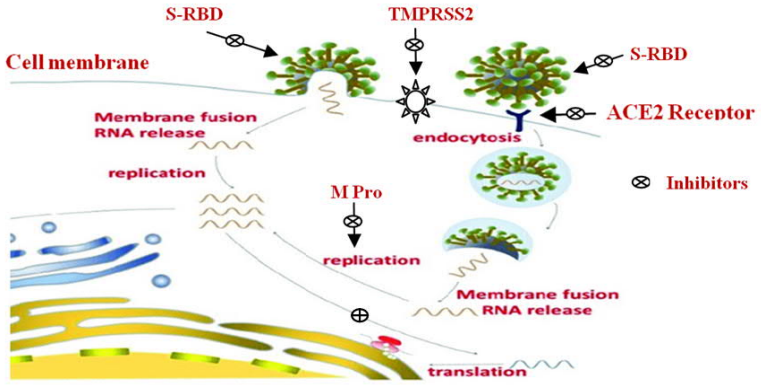

Figure 2. Membrane fusion and endocytosis mechanisms of viral cell entry showing potential receptor inhibitory sites: S-RBD, TMPRSS2, ACE2, M^{Pro} and translation

Bojkova [26] used quantitative translatome and proteome proteomics to obtain the cellular response to SARS-CoV-2 infection in human Caco-2 cells. Ribavirin (IC_{50} 0.07 mM), NMS-873 (0.025 μM), 2-deoxy-D-glucose (9.09 mM), pladienolide B (0.007 μM), cycloheximide (0.17 μM), emetine (0.47 μM), inhibited viral infection by interfering with translation, proteostasis, glycolysis, splicing and nucleotide synthesis pathways at concentrations that were not toxic to the Caco-2 cells. However the inhibitory efficacy of these drugs is dependent upon how well the drugs pass through the infected Caco-2 cell membrane.

Klann [27]studied SARS-CoV-2 infected Caco-2 cells and identified viral protein phosphorylation and phosphorylation-driven host cell signaling changes upon infection. Growth factor receptor signaling and downstream pathways are activated. Drug-protein network analyses revealed growth factor receptor signaling as a key target for viral inhibition by some approved anti-cancer drugs.

Study objectives:

(a) Develop a previously indentified LFER methodology based on quantum mechanical derived molecular descriptors to characterize the transport of a wide range of drugs into Caco-2 cells
(b) Identify how the ACE2 and TMPRSS2 surface receptors on the Caco-2 cells might influence drug transport into SARS-CoV-2 infected Caco-2 cells.
(c) Identify how various repurposed drugs can inhibit replication of M^{pro}, translation, proteonomics and growth factor signaling of SARS-CoV-2 infected Caco-2 cells.

Results

We have previously shown that the general equation 1 can successfully describe passive or facilitated diffusion transport processes of drugs across the cell membrane. [13-15]

Eq 1

$$\text{Drug Transport} = \Delta G_{desolv,CDS} + \Delta G_{lipo,CDS} + \text{Dipole Moment} + \text{Molecular Volume}$$

The four independent molecular specifiers in eq 1 can be useful in screening how drugs might be transported across the host cellular membrane or block the virus-host membrane interaction that is critical for progressing COVID-2019 infection.

Eq 2 can be applicable to the inhibition of the various proteases involved in the SARS-CoV-2, SARS-CoV and MERS-CoV replication process. We have previously shown [27-28] that the molecular specifiers used in eq 1 and eq 2 can be useful screening tools to evaluate the potential efficacy of therapeutic drugs that may be active against the SARS-CoV-2 virus.

Eq 2

Inhibition COVID-19 = $\Delta G_{desolv,CDS}$ + $\Delta G_{lipo,CDS}$ + Dipole Moment + Molecular Volume + HOMO-LUMO

where $\Delta G_{desolv,CDS}$ is the free energy of water desolvation, $\Delta G_{lipo,CDS}$ is the lipophilicity free energy in octane, DM is the dipole moment in water, Mol Vol is the molecular volume in water, and HOMO-LUMO is the energy gap in water.

(a) Permeability of drugs into Caco-2 cells

Analysis of P_{app}(AB) for Caco-2 cells from Yazdanian's study [6] for 52 widely structurally diverse drugs (see Table 1) is shown below in eq 3(a). Given the results of O'Hagan [5] who showed that active transporters may be the dominant form of transport across caco-2 cell membranes, the general form of eq 1 can be modified to include possible drug-carrier transporter interaction as identified by the HOMO-LUMO energy gap of the drugs, which reflect the $HOMO_{drug} \rightarrow LUMO_{transporter}$ molecular interaction, or the $HOMO_{transporter} \rightarrow LUMO_{drug}$.

Eq 3(a)

P_{app}(AB) = -0.35$\Delta G_{desolv,CDS}$ - 0.23$\Delta G_{lipo,CDS}$ -0.72DM - 0.024Mol Vol – 3.90(HOMO-LUMO) + 41.87

Where R^2 = 0.222, SEE = 10.59, SE($\Delta G_{desolvCDS}$) = 0.51, SE($\Delta G_{lipoCDS}$) = 0.87, SE(DM)= 0.29, SE(Mol Vol) = 0.034, SE(HOMO-LUMO) = 1.58, F=2.62, Significance= 0.036

It is clear that there is little significance in $\Delta G_{desolv,CDS}$, $\Delta G_{lipo,CDS,}$ or Mol Vol as judged by the large SE values and their corresponding P-values (0.50, 0.79, and 0.49 respectively), whereas the DM and HOMO-LUMO independent variables have P-values of 0.017 each. It should be noted that all the 52 diverse drugs have been included in the regression analysis, with no statistical optimization methods such as training sets and test sets or machine/artificial learning techniques etc which artificially optimize test data such as used in QSAR methods which seek to find relationships with *any* independent variables that might fit the data. [7,9] [Ponce, Santos-Filho] The correlation coefficient R^2 is a measure of the variability or scatter around the best fit regression line, whereas a low P-value for any independent variable indicates that the coefficient for that variable is statistically not zero (ie reject the null hypothesis that the coefficients are zero). The low P-values of 0.017 indicate that DM and the HOMO-LUMO in eq 3(a) are highly significant compared to the values for $\Delta G_{desolv,CDS}$, $\Delta G_{lipo,CDS}$ (for both n-octane and n-octanol) or Mol Vol at 0.50, 0.79 and 0.18, and 0.49 respectively. This LFER approach always uses the same 5 independent variables as molecular specifiers in seeking structure activity relationships.

No outliers were excluded in eq 3(a). The 52 drugs tested in eq 3(b) were the neutral forms only, but where charged forms were possible for 23 drugs, inclusion of these forms in addition to their neutral counterparts gave a very similar equation to eq 3(b) for the 75 neutral and charged drugs.

Eq 3(b) can be derived from eq 3(a) by eliminating the non-significant variables to give eq 3(b), which show that active transportation is the dominant mechanism based on the strong dependency on the dipole moment and HOMO-LUMO gap:

Eq 3(b)

$$\mathbf{P_{app}(AB) = -0.70DM - 3.64(HOMO\text{-}LUMO) + 38.75}$$

Where R^2 = 0.208, SEE = 10.35, SE(DM)= 0.28, SE(HOMO-LUMO) = 1.35, F=6.42, Significance= 0.0033

Analysis of the P_{app}(BA) for 17 drugs (see Table 1(a)) gives eq 4 with similar results as those shown in eq 3(b) with negligible dependencies on $\Delta G_{desolv,CDS}$, $\Delta G_{lipo,CDS}$ (both n-octane and n-octanol) or Mol Vol:

Eq 4

$$\mathbf{P_{app}(BA) = -1.76DM - 3.84(HOMO\text{-}LUMO) + 49.68}$$

Where R^2 = 0.463, SEE = 10.83, SE(DM)= 0.54, SE(HOMO-LUMO) = 2.46, F=6.04, Significance= 0.012

It is noted that 7 drugs have efflux ratio ER = $\{P_{app}(BA) / P_{app}(AB)\} > 2$, with another 8 having ER between 1-2, and two with ER <1 (caffeine and progesterone). Acebutolol 20.98 and chlorothiazide 13.89 have very large ERs. The ER data indicates significant involvement of apical efflux transporters, although the ER can also be dependent on passive permeability as well. [1,2] These ER ratios strongly support the HOMO-LUMO gap as being an indicator of active transport processes in Caco-2 cells, and the similarity between eqs 4 and 3(b) again indicate that active transport processes predominate in P_{app}(AB) and P_{app}(BA).

Analysis of Fredlund's data [24] (Table 2) for the permeability of 58 diverse neutral drugs in Caco-2 cells gives eq 5(a). P-values for $\Delta G_{desolv,CDS}$, $\Delta G_{lipo,CDS}$ (octanol) Mol Vol and HOMO-LUMO were 0.0015, 0.083, 0.00013, 0.010 were highly significant whereas the values for $\Delta G_{lipo,CDS}$ (octane) and DM were not significant 0.31 and 0.75. The molecular volume has been scaled by 30 times to allow direct comparison with the other coefficients. Eq 5(a) indicates that transcellular passive diffusion (dependency on $\Delta G_{desolv,CDS}$ and $\Delta G_{lipo,CDS}$ (octanol)), paracellular diffusion (dependency on molecular volume) and active transportation (dependency on the HOMO-LUMO gap) are all occurring.

Eq 5(a)

$$\mathbf{P_{app}(AB) = -4.71\Delta G_{desolv,CDS} - 2.71\Delta G_{lipo,CDS} - 5.25Mol\ Vol - 11.11(HOMO\text{-}LUMO) + 85.50}$$

Where R^2 = 0.288, SEE = 18.98, SE($\Delta G_{desolvCDS}$) = 1.40, SE($\Delta G_{lipoCDS}$) = 1.54, SE(Mol Vol) = 1.28, SE(HOMO-LUMO) = 4.19, F=5.36, Significance= 0.0010

Fredlund also measured the apparent intrinsic permeability P_{app}(AB) across Caco-2 cells of the same 58 drugs (Table 2) with a cocktail of chemical inhibitors of the three major efflux transporters ABCB1, ABCC2, and ABCG2. [24] The intrinsic P_{app} values were thought by

Fredlund to allow an estimate of passive permeability. The intrinsic P_{app} values are analyzed in eq 5(b). P-values for $\Delta G_{desolv,CDS}$, $\Delta G_{lipo,CDS}$ (octanol), Mol Vol and HOMO-LUMO were 0.0006, 0.063, 0.00011, 0.0055 were highly significant whereas the values for $\Delta G_{lipo,CDS}$ (octane) 0.31 and DM 0.90 were not significant.

Eq 5(b)

$$\textbf{Intrinsic } P_{app}\textbf{(AB)} = -6.83\Delta G_{desolv,CDS} - 3.91\Delta G_{lipo,CDS} - 7.14\text{Mol Vol} - 16.27(\text{HOMO-LUMO}) + 119.58$$

Where R^2 = 0.301, SEE = 25.45, SE($\Delta G_{desolvCDS}$) = 1.88, SE($\Delta G_{lipoCDS}$) = 2.06, SE(Mol Vol) = 1.71, SE(HOMO-LUMO) = 5.62, F=5.72, Significance= 0.00067

Fredlund's data set also includes the intrinsic permeability of 24 drugs (see Table 2) that were known to be actively transported by ABCB1, ABCC2, and ABCG2. These drugs are analyzed in eq 5(c), but are included in the 58 drugs tested in eq 5(b), so the remaining 34 drugs analyzed in eq 5(b) may or may not be transported by ABCB1, ABCC2, and ABCG2.

Eq 5(c) 24 drugs known to be transported by ABCB1, ABCC2, and ABCG2

$$\textbf{Intrinsic } P_{app}\textbf{(AB)} = -0.98\Delta G_{desolv,CDS} - 0.06\text{Mol Vol} - 2.66(\text{HOMO-LUMO}) + 33.46$$

Where R^2 = 0.290, SEE = 9.27, SE($\Delta G_{desolvCDS}$) = 0.78, SE(Mol Vol) = 0.023, SE(HOMO-LUMO) = 2.96, F=2.72, Significance= 0.071

However, the P-values for $\Delta G_{desolv,CDS}$, Mol Vol and HOMO-LUMO were 0.22, 0.015, 0.38, indicating that only the dependency on molecular volume is significant, as illustrated in eq 5(d):

Eq 5(d) 24 drugs known to be transported by ABCB1, ABCC2, and ABCG2 transporters

$$\textbf{Intrinsic } P_{app}\textbf{(AB)} = -0.040\text{Mol Vol} + 21.98$$

Where R^2 = 0.230, SEE = 9.27, SE(Mol Vol) = 0.015, F=6.54, Significance= 0.017=P-Value

Since transportation by the ABCB1, ABCC2, and ABCG2 transporters is known to occur for the 24 drugs in eqs 5(c) and 5(d), these results show that non-dependency on the HOMO-LUMO gap is an indicator of inhibition of active transport processes by the ABCB1, ABCC2, and ABCG2 transporters. And when that active transport ceases, the remaining transport process is dependent only on the molecular volume of the drugs, ie paracellular diffusion still occurs. It would be expected that transcellular diffusion would show some dependency on the lipophilicity $\Delta G_{lipo,CDS}$ as interaction must occur between the drug and the lipophilic Caco-2 cell membrane.

Li [23] has tested the "presumed" passive permeability of 19 drugs (see Table 3) in Caco-2 cells as analyzed in eq 6. It was found that P_{app}(AB) was only dependent on molecular volume when evaluated against P-values for all other independent variables $\Delta G_{desolv,CDS}$, $\Delta G_{lipo,CDS}$ (both octane and octanol), DM, and HOMO-LUMO gap. Eq 6 indicates that paracellular diffusion is the dominant transport mechanism.

Eq 6

$$\textbf{P}_{app}\textbf{(AB)} = -0.042\text{Mol Vol} + 21.12$$

Where R^2 = 0.422, SEE = 4.50, SE(Mol Vol) = 0.011, F=12.40, Significance= 0.0026=P-Value

Camenisch [12] found that the permeability of a diverse range of structurally different drugs (see Table 4) pass through Caco-2 cells by passive diffusion based on dependency on log $D_{octanol}$ and molecular weight (MW) of the 36 tested drugs. LFER analysis again found that permeability of 36 neutral drugs was only statistically dependent on the $\Delta G_{desolv,CDS}$, $\Delta G_{lipo,CDS}$ (octanol only), and molecular volume as shown in eq 7, as evaluated against P-values for all other independent variables $\Delta G_{desolv,CDS}$, $\Delta G_{lipo,CDS,}$ DM, and HOMO-LUMO gap. Interestingly no correlation was found with $\Delta G_{lipo,CDS}$ (octane) with a P-value of 0.68. P-values for $\Delta G_{desolv,CDS}$, $\Delta G_{lipo,CDS}$ (octanol), Mol Vol and HOMO-LUMO were 0.0020, 0.00001, and 0.00011 were highly significant. P-values for DM 0.31, HOMO-LUMO gap 0.42 and $\Delta G_{lipo,CDS}$ (octane) 0.58 were not significant. Eq 7 indicates that both transcellular (dependency on $\Delta G_{desolv,CDS}$ and $\Delta G_{lipo,CDS}$**)** and paracellular transport (dependency on molecular volume) processes are occurring concurrently. The molecular volume coefficient was multiplied by 35 to allow scaling comparisons with the $\Delta G_{desolvCDS}$ and $\Delta G_{lipoCDS}$ (octanol) coefficients. A strong correlation was found between the calculated $\Delta G_{lipoCDS}$ (octanol) and the experimental log $D_{octanol}$ for both 36 neutral and 11 charged species (see Materials and methods). Inclusion of 11 charged species to give 47 drugs tested gave a similar equation to eq 7, but it is assumed that the neutral species permeate faster than their charged equivalents, so eq 7 is the preferred model.

Eq 7

$$\mathbf{\log P_{app}(AB) = -0.28\Delta G_{desolv,CDS} - 0.33\Delta G_{lipo,CDS} -0.37 Mol\ Vol - 4.39}$$

Where R^2 = 0.516, SEE = 0.789**,** SE($\Delta G_{desolvCDS}$) = 0.083, SE($\Delta G_{lipoCDS}$) = 0.064, SE(Mol Vol) = 0.084, F=11.39, Significance= 0.00003

(b) SARS-CoV-2 infected Caco-2 cells: inhibition and drug transport into cells

Ellinger et al [25] investigated a collection of 5632 compounds including 3488 compounds which have undergone clinical investigations (marketed drugs, phases 1 -3, and withdrawn) for their inhibition of viral induced cytotoxicity using the human epithelial colorectal adenocarcinoma cell line Caco-2 and a SARS-CoV-2 isolate obtained from an individual originally exposed to the virus in the Wuhan region of China. A total of 64 compounds with IC_{50} <20 μM were identified in the primary screen, including 19 compounds with IC_{50} < 1 μM. ACE2 is expressed in Caco-2, Calu-3 and Vero-6 cells on the apical membrane domains. Primary screening was performed at 10μM compound concentration, at a virus multiplicity of infection (MOI) of 0.01 and a virus incubation period of 48 h, to ensure multiple viral replication cycles. It is thought that the assay procedure is able to confirm the activity of clinically relevant compounds against both viral entry and replication mechanisms. Remdesivir was found to show the same inhibition of SARS-CoV-2 in Caco-2 and Vero-6 cells (IC_{50} 0.77 μM), and interestingly, higher potency IC_{50} 0.07 μM in SARS-CoV and MERS.

Analysis of Ellinger's IC_{50} data for SARS-CoV-2 in Caco-2 cells [Fong 28,29] for 56 widely structurally diverse drugs is shown below in eq 8(a). No correlation was found with the dipole moment. The molecular volumes have been scaled by 35 times to allow a direct comparison of the relative magnitudes of the four molecular specifiers.

Eq 8(a)

$IC_{50} = 0.76\Delta G_{desolv,CDS} + 0.82\Delta G_{lipo,CDS} + 1.71$Mol Vol – 0.09(HOMO-LUMO) + 4.34

Where $R^2 = 0.174$, SEE = 5.55, SE($\Delta G_{desolvCDS}$) = 0.30, SE($\Delta G_{lipoCDS}$) = 0.34, SE(Mol Vol) = 0.54, SE(HOMO-LUMO) = 0.73, F=2.69, Significance= 0.041

It is clear that eq 8(a) shows a small dependency on the HOMO-LUMO gap, which can be eliminated to give eq 8(b) which is more significant by virtue of the elimination of the HOMO-LUMO variable:

Eq 8(b)

$IC_{50} = 0.76\Delta G_{desolv,CDS} + 0.83\Delta G_{lipo,CDS} + 1.71$Mol Vol + 4.34

Where $R^2 = 0.174$, SEE = 5.55, SE($\Delta G_{desolvCDS}$) = 0.30, SE($\Delta G_{lipoCDS}$) = 0.34, SE(Mol Vol) = 0.54, F=3.64, Significance= 0.018

It is noted that the P-values of the coefficients of the $\Delta G_{desolvCDS}$, $\Delta G_{lipoCDS}$ (octane) and Molecular Volume molecular specifiers in eq 8(b) are significant at 0.015, 0.018 and 0.003 levels. The low regression coefficient is partly due to the low sensitivity of the coefficients to IC_{50}, since the regression coefficient is dependent on the slope of the regression line. Eq 8(b) and 8(a) also includes 9 positively charged drugs and their neutral counterparts, since these drugs can be charged at neutral pH conditions in vitro. Eq 8 shows dependency on $\Delta G_{lipoCDS}$ (octane) but not with $\Delta G_{lipoCDS}$ (octanol) and no dependency on the HOMO-LUMO gap.

Analysis of the limited data of Bojkova [26] for the inhibition of SARS-CoV-2 infection in human Caco-2 cells by interfering with translation, proteostasis, glycolysis, splicing and nucleotide synthesis pathways showed that IC_{50} was highly correlated with the HOMO-LUMO gap or LUMO (but not HOMO) of the six inhibitors as per eq 9(a) or 9(b). No significant dependencies were found with the other independent variables. Both eq 9(a) or 9(b) indicate intracellular active processes are occurring.

Eq 9(a)

$IC_{50} = 2494.7$(HOMO-LUMO) - 13187

Where $R^2 = 0.897$, SEE = 1329.4, SE(HOMO-LUMO) = 422.5, F=34.84, Significance= 0.004=P-value

Eq 9(b)

$IC_{50} = 2880.9$(LUMO) + 2898.8

Where $R^2 = 0.850$, SEE = 1607.4, SE(LUMO) = 606.4, F=22.6, Significance= 0.009=P-value

Analysis of the limited data (5) of Klann [27] for the inhibition of SARS-CoV-2 infected Caco-2 cells by inhibition of growth factor receptor signaling gives eq 10. No dependencies were found with HOMO, or HOMO-LUMO, or the other independent variables $\Delta G_{desolv,CDS}$, $\Delta G_{lipo,CDS}$, Dipole Moment, or Mol Vol. Eq 10 indicates intracellular active processes are occurring.

Eq 10

$IC_{50} = 5.47$(LUMO) + 10.94

Where $R^2 = 0.946$, SEE = 0.54, SE(LUMO) = 0.64, F=71.2, Significance= 0.0035=P-value

Eqs 9(b) and 10 are very similar inhibitory studies of mechanism of virus replication processes in infected Caco-2 cells.

(c) In vitro and docking binding energies of SARS-CoV-2 inhibition: M^{pro}, ACE2, S-RBD, TMPRSS2

We have previously shown Fong [28,29] that using the same LFER methodology, stepwise analysis of 23 inhibitors from Vatansever [30] of the M^{pro} of SARS-CoV-2 yields eq 11. It is noted that the p-values of the coefficient of the HOMO-LUMO molecular specifier is modestly significant at the 0.077 level.

Eq 11

$$\mathbf{IC_{50} = 64.71(HOMO\text{-}LUMO) + 60.40}$$

Where R^2 = 0.14, SEE = 189.96, SE(HOMO-LUMO) = 34.84, F=3.49, Significance=0.077

Molecular docking is currently the mainstay of predictive computational methods to evaluate new and repurposed ant-virals for coronaviruses, and there have been some reports [30,31] that inhibitory structure activity relationships (SARs) do not always agree with docking results for the M^{pro}. Analysis of the docking binding energy of 22 inhibitors to M^{pro} (PDB 6LU7) from Vatansever [30] was previously shown by Fong [28,29] to give eq 12. It is noted that the corresponding correlation with HOMO is much poorer than that for LUMO in eq 12, and the dependencies on the other independent variables were poor.

Eq 12

$$\mathbf{Docking\ Binding\ Energy = 0.58LUMO - 8.72}$$

Where R^2 = 0.31, SEE = 0.75, SE(LUMO) = 0.19, F=8.65, Significance=0.008

It can be seen that in vitro IC_{50} inhibitory assay studies in eq 11 are related to the theoretical docking binding energies in eq 12, but not directly related for this series of drugs, since eq 11 shows a dependency on the HOMO-LUMO gap whereas eq 12 is more strongly correlated to the LUMO only. Importantly, the experimental in vitro inhibition IC_{50} of the these drugs is directly related to the calculated docking binding energy through the HOMO-LUMO gap in eq 11 or the closely related LUMO in eq 12.

Fischer et al [32] computationally screened a library of over 606 million compounds for binding to the main protease (M^{pro}) of SARS-CoV-2 (PDB 6LU7) and identified 15 repurposed potential inhibitors of the M^{pro}. We have previously shown [28,29] that eq 13 is the best correlation.

Eq 13

$$\mathbf{Docking\ BE\ (M^{pro}) = -2.63\Delta G_{desolv,CDS} + 3.93\Delta G_{lipo,CDS} - 5.68HOMO\text{-}LUMO - 30.76}$$

Where R^2 = 0.561, SEE = 7.47, SE($\Delta G_{desolvCDS}$) = 1.02, SE($\Delta G_{lipoCDS}$) = 1.09, SE(HOMO-LUMO) = 5.11, F=4.69, Significance=0.024

It can be seen that the docking binding energies to M^{pro} are related to the molecular specifiers of the inhibitors used in eqs 11 and 12, but the HOMO-LUMO or LUMO are the dominant factors influencing the binding energies.

We have previously shown [28,29] Fong] that docking studies of the angiotensin-converting enzyme 2 (ACE2) receptor can also be used to derive structural activity LFER relationships. Terali has investigated the binding of 9 repurposed drugs [33] to the ACE2 receptor eq 14:

Eq 14

Docking BE (ACE2) = -0.81HOMO - 0.18 Molecular Volume - 8.16

Where R^2 = 0.52, SEE = 0.45, SE(HOMO) = 0.56, SE(Molec Vol) = 0.09, F=3.27, Significance=0.109

Using Choudhary's molecular docking binding energy [34] of 10 drugs to the ACE2 receptor gives eq 15;

Eq 15

Binding Energy (ACE2) = -1.14$\Delta G_{lipo,CDS}$ - 0.58Mol Vol - 8.35HOMO – 64.72

Where R^2 = 0.73, SEE = 1.42, SE($\Delta G_{lipoCDS}$) = 0.33, SE(Mol Vol) = 0.30, SE(HOMO)= 3.08 , F=5.29, Significance= 0.040

Similarly using Choudhary's molecular docking binding energy [34] of 6 drugs to the SARS-CoV-2 receptor binding domain of the virus spike protein (S-RBD) gives eq 16(a) or 16(b);

Eq 16(a)

Binding Energy (S-RBD) = 2.585HOMO + 6.83

Where R^2 = 0.958, SEE = 0.22, SE(HOMO)= 0.27 , F=90.98, Significance= 0.00067

Eq 16(b) including $\Delta G_{lipo,CDS}$ and molecular volume gives:

Binding Energy (S-RBD) = 0.11$\Delta G_{lipo,CDS}$ + 0.15Mol Vol + 2.845HOMO + 8.66

Where R^2 = 0.981, SEE = 0.21, SE($\Delta G_{lipoCDS}$) = 0.075, SE(Mol Vol) = 0.01, SE(HOMO)= 0.32 , F=33.68, Significance= 0.029

Comparison of eqs 14 or 15 for the ACE2 binding energy and 16(b) for the S-RBD binding energy shows a reversal of sign for the three independent variables with far greater opposite dependence on the HOMO in eqs 14 or 15 compared to eq 16(b). These eqs indicate a substantial difference between the inhibitor binding interactions of the viral S-RBD and the ACE2.

Analysis of Smith's data [34] which is a computational model of the RBD of the spike protein (S-protein) of SARS-CoV-2 interacting with the human ACE2 receptor, for 14 repurposed inhibitors interacting with the S-protein of SARS-CoV-2 and the ACE2 receptor gives eq 17. [28,29] This result is unusual in this study as there is no dependency on the HOMO-LUMO gap, when the inhibitors interact with the ACE2 and S-RBD receptor.

Eq 17

Docking BE (ACE2+S-RBD) = -0.40$\Delta G_{lipo,CDS}$ + 0.017Dipole Moment - 7.50

Where R^2 = 0.462, SEE = 0.107, SE($\Delta G_{lipoCDS}$) = 0.016, SE(DM) = 0.007, F=4.71, Significance=0.033

The transmembrane serine 2 protease (TMPRSS2) on the cell surface is involved in S protein priming in lung cells, particularly involving the ACE2 receptor which is the main entry point into host cells for the SARS-Cov-2 virus. [28,29] Analysis of Roomi's docking of 24 repurposed drugs [36] to the TMPRSS2 receptor gives eqs 18(a) or (b):

Eq 18(a)

Docking BE (TMPRSS2) = -2.26LUMO - 0.43 Molecular Volume - 10.64

Where R^2 = 0.658, SEE = 1.07, SE(LUMO) = 0.57, SE(Molec Vol) = 0.16, F=20.20, Significance=0.00001

Eq 18(b) eliminating the weaker molecular volume specifier gives:

Docking BE (TMPRSS2) = -2.97LUMO - 13.87

Where R^2 = 0.547, SEE = 1.20, SE(LUMO) = 0.58, F=26.55, Significance=0.00003

We have previously shown [28,29] that analysis of the binding energy of 10 inhibitors of TMPRSS2 from Idris [37] gives eqs 19(a) or (b):

Eq 19(a)

Docking BE (TMPRSS2) = 1.09HOMO-LUMO - 0.49 Molecular Volume - 10.64

Where R^2 = 0.715, SEE = 0.85, SE(HOMO-LUMO) = 0.62, SE(Molec Vol) = 0.38, F=8.75, Significance=0.012

Eq 19(b)

Docking BE (TMPRSS2) = 1.67HOMO-LUMO – 15.00

Where R^2 = 0.649, SEE = 0.88, SE(HOMO-LUMO) = 0.62, F=14.77, Significance=0.005

Discussion

This study has shown that our LFER methodology based on quantum mechanical derived molecular descriptors can successfully describe: (a) the transport of a wide range of drugs into Caco-2 cells (as described by eqs 3-7) (b) the inhibition of SARS-CoV-2 infected Caco-2 cells (as described by eqs 8-10) and (c) in vitro inhibition and docking binding energies of SARS-CoV-2 of M^{pro}, ACE2, S-RBD, TMPRSS2 (as described by eqs 11-18). These equations were derived from applying the general form equation 2 to a large variety of inhibitors to find which of the five molecular specifiers can describe the transport of drugs into Caco-2 cells, or the inhibition of SARS-CoV-2 infected Caco-2 cells, or the in vitro inhibition or docking binding of inhibitors to the SARS-CoV-2 virus to host cells. It is noted that we have found that $\Delta G_{lipo,CDS}$ (octanol) better describes the lipophilicity of the Caco-2 cell membrane rather the $\Delta G_{lipo,CDS}$ (octane) molecular descriptor as previously identified. [12,16,28,29] However we have used $\Delta G_{lipo,CDS}$ (octane) to describe the lipophilicity involved in drug-receptor binding as usual as in eqs 11-18.

(a) Permeability of drugs into Caco-2 cells

It has been shown that apical to basolateral (AB) permeability, P_{app}(AB) for Caco-2 cells for 52 widely structurally diverse drugs (from the Yazdanian data [6]) and the basolateral to apical (BA) permeability P_{app}(BA) for 17 drugs are mainly dependent on the HOMO-LUMO gap and to a lesser extent, the dipole moments of the drugs, as shown in eq 3(a), 3(b) and 4. It is also noteworthy that eq 3(b) for the P_{app}(BA) data is very similar to that for P_{app}(AB), and apical efflux transport is well established in Caco-2 cells (see Figure 1). [1] Of the 17 drugs used to derive P_{app}(BA) in eq 4, 7 drugs have efflux ratio ER = {P_{app}(BA) / P_{app}(AB)} > 2, with another 8 having ER between 1-2, and two with ER <1 (caffeine and progesterone). Acebutolol 20.98 and chlorothiazide 13.89 have very large ERs. These ER data indicates significant involvement of apical efflux transporters, although the ER is also dependent on passive permeability as well.

Eqs 5(a) and (b) from Fredlund's data [24] describes the permeability P_{app}(AB) and the apparent intrinsic permeability P_{app}(AB) of the same 58 drugs with a cocktail of chemical inhibitors of the three major efflux transporters ABCB1, ABCC2, and ABCG2. It is seen that both equations show strong parallel dependencies on $\Delta G_{desolv,CDS}$, $\Delta G_{lipo,CDS}$, Mol Vol and the HOMO-LUMO gap.

Eq 5(d) for the intrinsic permeability of the 24 drugs known to be transported by ABCB1, ABCC2, and ABCG2 shows only a dependency on the molecular volume. The non-dependency on the HOMO-LUMO gap is an indicator of inhibition of active transport processes by the ABCB1, ABCC2, and ABCG2 transporters, and that when active transport ceases, the remaining transport process is dependent on the molecular volume of the drugs, ie paracellular diffusion then occurs. It would be expected that transcellular diffusion would show some dependency on the lipophilicity $\Delta G_{lipo,CDS}$ as interaction must occur between the drug and the lipophilic Caco-2 cell membrane.

It appears that eqs 5(a) and (b) describe (i) transcellular passive diffusion (dependency on $\Delta G_{desolv,CDS}$ and $\Delta G_{lipo,CDS}$), (ii) paracellular diffusion (dependency on molecular volume) and (iii) active transport (dependency on the HOMO-LUMO energy gap. These three processes can operate concurrently.

The dependency on the HOMO-LUMO gap directly indicates electronic interaction between the HOMO and LUMO of the drugs and some membrane transporter, ie $HOMO_{drug} \rightarrow LUMO_{transporter}$ and $HOMO_{transporter} \rightarrow LUMO_{drug}$. A passive transport process would not show such large associations with the HOMO-LUMO gap. This finding is broadly aligned with the previous finding by O'Hagan that most drugs enter (and exit) Caco-2 cells via a multiplicity of transporters of comparatively weak specificity. [5]

Eq 6 describes the "presumed" passive permeability of 19 drugs from [23] in Caco-2 cells where P_{app}(AB) was only dependent on molecular volume. This result indicates that paracellular diffusion predominates in this cell line.

Camenisch [12] found that the permeability of a diverse range of structurally different drugs pass through Caco-2 cells by passive diffusion based on dependency on log $D_{octanol}$ and molecular

weight (MW) of the 36 tested drugs. Eq 7 shows that permeability was only statistically dependent on the $\Delta G_{desolv,CDS}$, $\Delta G_{lipo,CDS}$ (octanol only), and molecular volume. This result is in broad agreement with the finding of Camenisch. It is noted that no dependency was found with the HOMO-LUMO gap, nor $\Delta G_{lipo,CDS}$ (octane). This result is consistent with both transcellular and paracellular diffusion occurring together.

In summary from eqs 3-7, dependency on the HOMO-LUMO gap indicates that permeability is an indication of active transportation, but in some studies only passive transcellular or paracellular permeation is found. This appears to suggest that different cell lines of CACo-2 may involve different or reduced transporters being present in the various drug permeation studies. Octanol (with better hydrogen bonding capability) is clearly a better proxy to describe the lipophilicity of the cell membrane than octane (no hydrogen bonding ability). P-values can be used to predict which molecular specifiers are statistically dominant in describing cell membrane transportation processes, however where multiple processes such as transcellular, paracellular, or active transportation may be occurring concurrently for a given series of drugs, then the correlation coefficient will reflect significant dispersion about the best fit relationships found in equations 3-7. This LFER methodology can quantitatively differentiate between passive transcellular, paracellular and active transport of drugs into Caco-2 cells.

(b) SARS-CoV-2 infected Caco-2 cells: inhibition and drug transport into cells

In this study, three cases of inhibition of SARS-CoV-2 infected Caco-2 cells are reported in eq 8(a), 8(b), 9(a), 9(b) and 10. Eqs 8(a) and (b) are derived from data that includes inhibitors that affect cellular entry of the virus (ACE2, TMPRSS2 and possibly S-RBD) or possibly intracellular processes such as inhibition of viral replication via M^{pro}. [25] Eq 9(a) and (b) and 10 are derived from inhibition of *intracellular* translation and growth factor receptor signaling processes in virus infected Caco-2 cells. [26,27] Eqs 9(a), 9(b), and 10 show strong IC_{50} linear dependencies on HOMO-LUMO or LUMO only, and we have shown that drugs are actively transported across the cell membrane have a strong dominant dependency on the HOMO-LUMO gap. It follows that the HOMO-LUMO gap or LUMO are strong predictors of how certain drugs can enter Caco-2 cells and inhibit virus infected internal cell replicative processes. It then is possible that *Ellinger's results* analyzed in eq 8(b) which show dependencies on $\Delta G_{desolvCDS,}$ $\Delta G_{lipoCDS}$ (octane) and molecular volume and negligible dependency on HOMO-LUMO appear to be a result of mainly *inhibition of Caco-2 cell entry processes involving ACE2, TMPRSS2 or S-RBD*, rather than intracellular inhibitory processes. This notion is further discussed below and in eq 17 where Smith's docking study [35] of inhibitors to the combined S-RBD and ACE2 binding pocket showed no dependence on the HOMO-LUMO gap, only dependency on the lipophilicity and dipole moment of the inhibitors.

(c) In vitro and docking binding energies of SARS-CoV-2 inhibition: M^{pro}, ACE2, S-RBD, TMPRSS2

It is clear that the application of the LFER model to the in vitro inhibition of (a) M^{pro} of SARS-CoV-2, (b) SARS-CoV-2 spike protein S-RBD, (c) ACE2 receptor, and the (d) TMPRSS2 receptor is well described over a wide range of repurposed drugs, as shown in eqs 11-19. [28,29] These results cover experimental IC_{50} studies and computational docking binding energy/affinity studies. The overwhelming conclusion is that the HOMO, or LUMO or the HOMO-LUMO energy gap of the various inhibitors is the principal determinant of inhibition of M^{pro} as well as the S-RBD of the virus or the binding interaction between the inhibitors and the host cell targets, ACE2 and TMPRSS2.

Eqs 17 derived from Smith's docking analysis [35] of the inhibition of the S-protein of SARS-CoV-2 interacting with the human {ACE2-S-RBD} combined receptor is an exception to the rule that HOMO, or LUMO or HOMO-LUMO is the principal determinant(s) of the binding energy. It is unclear whether this result is due to the interface between the S-protein and the ACE2 being a "shallow" binding pocket as opposed to the usual "buried" binding pocket, or possibly due to counterposing contributions from $inhibitor_{HOMO} \rightarrow receptor_{LUMO}$ or $receptor_{HOMO} \rightarrow inhibitor_{LUMO}$ dominated interactions for both S-protein and ACE2. The latter postulate is likely correct since we have shown that the binding of inhibitors to the ACE2 receptor (eqs 14 or 15) show a *negative* dependency on the HOMO, whereas binding of inhibitors to the S-RBD (eq 16) shows a *positive* dependency on the HOMO.

Conclusions

Detailed studies of the permeability of a very wide range of drugs into Caco-2 cells shows that active transport, passive transcellular and passive paracellular transport can be separately identified using the LFER method involving $\Delta G_{desolv,CDS}$, $\Delta G_{lipo,CDS}$ (both octane and octanol), dipole moment, molecular volume, and HOMO-LUMO gap. Active transport is dependent on the HOMO-LUMO energy gap. Transcellular passive permeability shows dependency on the cell membrane lipophilicity as measured by $\Delta G_{lipo,CDS}$ in n-octanol and the free energy of water desolvation $\Delta G_{desolv,CDS}$. Paracellular passive permeability shows dependency on the molecular volume in water. There is evidence that different Caco-2 cell lines in various literature permeability studies can result in varying contributions of active and passive transport modes for a given range of drugs.

Inhibition of SARS-CoV-2 infected Caco-2 cells can be studied using the LFER method to separate Caco-2 cell entry processes involving ACE2, TMPRSS2 or S-RBD from intracellular inhibitory processes. The extensive study by Ellinger [25] likely predominantly involves the inhibition of Caco-2 cell entry processes involving ACE2, TMPRSS2 or S-RBD. It is known that Caco-2 cells were the only human cell type of 13 tested refractory cell lines that supported efficient SARS-CoV replication and expression of the SARS-CoV receptor, ACE2, [38] and Chu [39] found both human Calu-3 cells and Caco-2 cells were best suited for studying SARS-CoV-2 replication. Ellinger's data for Caco-2 cells is a valuable source for evaluating the efficacy of SARS-CoV-2 therapeutics.

The in vitro IC_{50} and docking binding energies of SARS-CoV-2 inhibition of M^{pro}, ACE2, S-RBD, TMPRSS2 show that the overwhelming conclusion is that the HOMO, or LUMO or the HOMO-LUMO energy gap is the principal determinant of inhibition of M^{pro}, S-RBD, ACE2 and TMPRSS2. The exception to this rule is the inhibitory binding to the human {ACE2-S-RBD} combined receptor which is likely to be a result of counterposing contributions from $inhibitor_{HOMO} \rightarrow receptor_{LUMO}$ or $receptor_{HOMO} \rightarrow inhibitor_{LUMO}$ dominated interactions for both S-protein and ACE2.

Materials and methods

All calculations were carried out using the Gaussian 09 package. Energy optimizations were at the DFT/B3LYP/6-31G(d) (6d, 7f) level of theory for all atoms in water. Selected optimizations at the DFT/B3LYP/6-311+G(d,p) (6d, 7f) level of theory gave very similar results to those at the lower level. Optimized structures were checked to ensure energy minima were located, with no imaginary frequencies. Energy calculations were conducted at the DFT/B3LYP/6-31G(d,p) (6d, 7f) for neutral and cationic compounds with optimized geometries in water, using the IEFPCM/SMD solvent model. With the 6-31G* basis set, the SMD model achieves mean unsigned errors of 0.6 - 1.0 kcal/mol in the solvation free energies of tested neutrals and mean unsigned errors of 4 kcal/mol on average for ions. [39] The 6-31G** basis set has been used to calculate absolute free energies of solvation and compare these data with experimental results for more than 500 neutral and charged compounds. The calculated values were in good agreement with experimental results across a wide range of compounds. [40,41] Adding diffuse functions to the 6-31G* basis set (ie 6-31+G**) had no significant effect on the solvation energies with a difference of less than 1% observed in solvents, which is within the literature error range for the IEFPCM/SMD solvent model. HOMO and LUMO calculations included both delocalized and localized orbitals (NBO). It is noted that high computational accuracy for each species in different environments is not the focus of this study, but comparative differences between various species is the aim of the study. Experimental errors in inhibitory and docking binding studies are substantially higher than those for calculated molecular specifiers.

Additional data related to eq 7: The relationship $\Delta G_{lipo,CDS}$ (octanol) = -0.63 logD + 1.15 where SE=1.95, F=14.54, significance 0.0005 was found for the experimental log D for 36 neutral species from ref 12, or by including 11 charged species in addition to the 36 neutral species $\Delta G_{lipo,CDS}$ (octanol) = -0.705 logD + 1.23 where SE=2.05, F=23.20, significance 0.00005. The relationship $\Delta G_{lipo,CDS}$ (octanol) = $\Delta G_{lipo,CDS}$ (octane) + 2.345 where SE=2.25, F=2.28, significance 0.14 for 36 neutral species was far weaker.

References

[1] H Sun, ECY Chow, S Liu, Y Du, K Sandy Pang, The Caco-2 cell monolayer: usefulness and limitations, Expert Opin. Drug Metab. Toxicol. 2008, 4, 395-411
[2] H Pham-The, MA Cabrera-Pérez, NH Nam, In silico assessment of ADME properties: Advances in Caco-2 Cell Permeability Modeling, Curr Topics Med Chem, 2018, 18, 2209-2229
[3] K Lanevskij, R Didziapetris, Physicochemical QSAR Analysis of Passive Permeability Across Caco-2 Monolayers, J Pharm Sci 2019, 108, 78-86

[4] JB Lee, A Zgair, DA Taha DA, et al, Quantitative analysis of lab-to-lab variability in caco-2 permeability assays, Eur J Pharm Biopharm, 2017, 114, 38-42.
[5] S O'Hagan, DB Kell, The apparent permeabilities of Caco-2 cells to marketed drugs: magnitude, and independence from both biophysical properties and endogenite similarities, Peer J 3:e1405, 2015, DOI 10.7717/peerj.1405
[6] M Yazdanian, SL Glynn, JL Wright, A Hawi, Correlating partitioning and Caco-2 cell permeability of structurally diverse small molecular weight compounds, Pharm Res, 1998, 15, 1490-1494.
[7] YM Ponce, MA Cabrera Pérez, VR Zaldivar, et al, A new topological descriptors based model for predicting intestinal epithelial transport of drugs in caco-2 cell culture, J Pharm Pharmaceut Sci 2004, 7, 186-199
[8] E Milanetti1, D Raimondo, A Tramontano, Prediction of the permeability of neutral drugs inferred from their solvation properties, Bioinformatics, 2016, 32,1163–1169.
[9] OA Santos-Filho, AJ Hopfinger, Combined 4D-Fingerprint and Clustering Based Membrane-Interaction QSAR Analyses for Constructing Consensus Caco-2 Cell Permeation Virtual Screens, J Pharm Sci, 2008, 97, 566-583
[10] DS Kim, PS Burton, RT Borchardt, A correlation between the permeability of a series of peptides using an in vitro cell culture model Caco-2 and those using an in situ perfused rat ileum culture model of the intestinal mucosa, Pharm Res 1993, 10, 1710-15
[11] CM Van Itallie, J Holmes, A Bridges, JL Gookin, et al, The density of small tight junction pores varies among cell types and is increased by expression of claudin-2, J Cell Sci, 2008, 121, 298-305
[12] G Camenisch, J Alsenz, H van de Waterbeemd, G Folkers, Estimation of permeability by passive diffusion through Caco-2 cell monolayers using the drugs' lipophilicity and molecular weight, Eur J Pharm Sci 1998, 6, 317-24
[13] CW Fong, Permeability of the Blood–Brain Barrier: Molecular Mechanism of Transport of Drugs and Physiologically Important Compounds, J Membr Biol. 2015, 248,651-69.
[14] CW Fong, The extravascular penetration of tirapazamine into tumours: a predictive model of the transport and efficacy of hypoxia specific cytotoxic analogues and the potential use of cucurbiturils to facilitate delivery, Int J Comput Biol Drug Design. 2017, 10, 343-373
[15] CW Fong, Statins in therapy: Understanding their hydrophilicity, lipophilicity, binding to 3-hydroxy-3-methylglutaryl-CoA reductase, ability to cross the blood brain barrier and metabolic stability based on electrostatic molecular orbital studies. Eur J Med Chem. 2014, 85, 661-674
[16] Balaz S. Modelling kinetics of subcellular disposition of chemicals, Chem. Revs., 2009, 109, 1753.
[17] K Palm, K Luthman, J Ros, J Grasjo, P Artursson, Effect of molecular charge on intestinal epithelial drug transport: pH-dependent transport of cationic drugs, J Pharmacol Exp Ther, 1999, 29, 435-443.
[18] S Neuhoff, AL Ungell, I Zamora, P Artursson, pH-dependent bidirectional transport of weakly basic drugs across caco-2 monolayers: implications for drug-drug interactions, Pharm Res, 2003, 20, 1141-1148.
[19] S Neuhoff, AL Ungell, I Zamora, P Artursson, pH-Dependent passive and active transport of acidic drugs across caco-2 cell monolayers. Eur J Pharm Sci, 2005, 25, 211-220.

[20] KJ Lee, N Johnson, J Castelo, et al, Effect of experimental pH on the in vitro permeability in intact rabbit intestines and Caco-2 monolayer, Eur J Pharm Sci, 2005, 25, 193–200
[21] Y Mimura, T Yasujima, K Ohta, K Inoue, H Yuasa, Functional identification of organic cation transporter 1 as an atenolol transporter sensitive to flavonoids, Biochem Biophys Rep, 2015, 2, 166-171
[22] P Dixit, DK Jain, J Dumbwani, Standardization of an ex vivo method for determination of intestinal permeability of drugs using everted rat intestine apparatus, J Pharmacol Toxicol Methods, 2012, 65, 13-17.
[23] N Li , Z Sui, Y Liu, D Wang, G Ge, L Yang, A fast screening model for drug permeability assessment based on native small intestinal extracellular matrix, RSC Adv., 2018, 8, 34514-34524
[24] L Fredlund, S Winiwarter, C Hilgendorf, In Vitro Intrinsic Permeability: A Transporter-Independent Measure of Caco-2 Cell Permeability in Drug Design and Development, Mol. Pharmaceutics 2017, 14, 1601–1609
[25] B Ellinger, D Bojkova, A Zaliani et al, Identification of inhibitors of SARS-CoV-2 in-vitro cellular toxicity in human (Caco-2) cells using a large scale drug repurposing collection, Research Square, 2020, doi: 10.21203/rs.3.rs-23951/v1
[26] D Bojkova, K Klann, B Koch, et al, Proteomics of SARS-CoV-2-infected host cells reveals therapy targets, Nature, 2020, 583, 469-485
[27] K Klann, D Bojkova, G Tascher, et al, Growth Factor Receptor Signaling Inhibition Prevents SARS-CoV-2 Replication, Molecular Cell 2020, 80, 164–174
[28] CW Fong, COVID-19: Covid-19: Predicting inhibition of SARS-CoV-2 in Caco-2 cells: viral cellular entry, hal archives 2020, hal-02943341v1
[29] CW Fong, COVID-19: Predicting inhibition of repurposed drugs for SARS-CoV-2 viral activity and cellular entry, hal archives 2020, hal-02963306v1
[30] EC Vatansever, K Yang, KC Kratch, A Drelich, et al, Targeting the SARS-CoV-2 Main Protease to Repurpose Drugs for COVID-19, bioRxiv Preprint 2020 Jul 27, doi: 10.1101/2020.05.23.112235
[31] T Bobrowski, V Alves, CC Melo-Filho, et al, Computational Models Identify Several FDA Approved or Experimental Drugs as Putative Agents Against SARS-CoV-2, ChemRxiv 2020 Preprint https://doi.org/10.26434/chemrxiv.12153594.v1
[32] A Fischer, M Sellner, S Neranjan, M Smieško, MA Lill, Potential Inhibitors for Novel Coronavirus Protease Identified by Virtual Screening of 606 Million Compounds, Int J Mol Sci 2020, 21, 3626; doi:10.3390/ijms21103626
[33] K Terali, B Baddal, HO Gülcan, Prioritizing potential ACE2 inhibitors in the COVID-19 pandemic: Insights from a molecular mechanics-assisted structure-based virtual screening experiment, J Molec Graph Model, 2020, 100, 107697-107707
[34] S Choudhary, YS Malik, S Tomar, Identification of SARS-CoV-2 Cell Entry Inhibitors by Drug Repurposing Using *in silico* Structure-Based Virtual Screening Approach, Front. Immunol., 2020, https://doi.org/10.3389/fimmu.2020.01664
[35] M Smith, JC Smith, Repurposing Therapeutics for COVID-19: Supercomputer-Based Docking to the SARS-CoV-2 Viral Spike Protein and Viral Spike Protein-Human ACE2 Interface. ChemRxiv. 2020, Preprint. https://doi.org/10.26434/chemrxiv.11871402.v4

[36] MS Roomi, YD Khan, Potential Compounds for the Inhibition of TMPRSS2, 2020, https://doi.org/10.26434/chemrxiv.12727787.v1
[37] MO Idris , AA Yekeen , OS Alakanse, OA Durojaye, Computer-aided screening for potential TMPRSS2 inhibitors: a combination of pharmacophore modeling, molecular docking and molecular dynamics simulation approaches, J Biomol Struct Dyn, DOI: 10.1080/07391102.2020.1792346
[38] EC Mossel, C Huang, K Narayanan, S Makino, RB Tesh, CJ Peters, Exogenous ACE2 Expression Allows Refractory Cell Lines To Support Severe Acute Respiratory Syndrome Coronavirus Replication, J Virology, 2005, 79, 3846-50
[39] H Chu, JF-W Chan, TT-T Yuen, et al. Comparative tropism, replication kinetics, and cell damage profiling of SARS-CoV-2 and SARS-CoV and implications for clinical manifestations, transmissibility, and laboratory studies of COVID-19: an observational study, Lancet Microbe 2020; published online April 21. https://doi.org/S2666-5247(20)30004-5.
[40] AV Marenich, CJ Cramer, DJ Truhlar, Universal Solvation Model Based on Solute Electron Density and on a Continuum Model of the Solvent Defined by the Bulk Dielectric Constant and Atomic Surface Tensions, J Phys Chem B, 2009, 113, 6378 -96
[41] S Rayne, K Forest, Accuracy of computational solvation free energies for neutral and ionic compounds: Dependence on level of theory and solvent model, Nature Proceedings, 2010, http://dx.doi.org/10.1038/npre.2010.4864.1.
[42] RC Rizzo, T Aynechi, DA Case, ID Kuntz, Estimation of Absolute Free Energies of Hydration Using Continuum Methods: Accuracy of Partial Charge Models and Optimization of Nonpolar Contributions, J Chem Theory Comput. 2006, 2, 128-139

Table 1. P_{app}(AB) for Caco-2 cells [6] for 52 widely structurally diverse drugs: eq 3(b)

	P(AB) 10^-6 cm/s	$\Delta G_{desolv,CDS}$ kcal/mol	$\Delta G_{lipo,CDS}$ octanol kcal/mol	Dipole Moment D	Molec Volume cm^3/mol	HOMO-LUMO gap eV
Aminopyrine	36.5	-5.4	-0.12	6.93	173	5.07
Caffeine	30.8	-5.29	0.74	5.7	126	5.04
Nevirapine	30.1	-4.04	-1.07	3.67	216	4.33
Phenytoin	26.7	-7.39	1.08	3.75	175	5.72
Testosterone	24.9	-6.27	-1.9	4.98	212	5.29
Phencyclidine	24.7	-3.64	-4.29	1.26	218	5.48
Desipramine	24.4	-3.74	-3.66	2.35	209	5.05
Progesterone	23.7	7.51	-1.48	7.61	280	5.23
Clonidine	21.8	-0.44	-3.69	2.97	151	5.11
Propranolol	21.8	-4.64	-1.75	4.14	206	4.74
Chlorpromazine	19.9	-2.87	-4.28	2.96	271	4.44
Meloxicam	19.5	-7.24	2.67	17.55	257	3.57
Nicotine	19.4	-0.99	-1.71	3.19	133	5.23
Pindolol	16.7	-4.79	-0.78	4.31	200	5.22
Telmisartan	15.1	-7.91	-3.26	3.2	335	4.10

Hydrocortisone	14	-8.54	-0.07	12.1	276	5.30
Timolol	12.8	-2.53	-1.36	2.9	241	4.53
Scopolamine	11.8	-4.21	-0.73	1.99	198	5.50
Scopolamine Ion	11.8	-7.16	-0.08	18.49	253	6.35
Dopamine	9.33	-3.3	0.64	3.09	124	5.79
Labetalol	9.31	-6.95	-0.19	10.72	240	4.98
Bremazocine	8.02	-5.96	-2.04	1.62	284	5.43
Urea	4.56	-3.48	2.46	6.13	54	8.81
Uracil	4.24	-5.11	2.89	6.43	69	5.65
Cimetidine	1.37	-4.6	-3.18	4.05	184	6.26
Methyl Scopolamine Ion	0.69	-7.71	0.15	15.88	248	6.24
Hydrochlorothiazide	0.51	-2.64	3.15	13.5	167	4.92
Acebutolol	0.51	-8	0.69	7.11	282	4.30
Ranitidine	0.49	-5.04	0.26	15.49	241	4.05
Pirenzepine	0.44	2.28	-1.45	8.09	250	4.42
Mannitol	0.38	-4.76	2.27	3.38	137	8.99
Sulfasalazine	0.3	-6.85	3.76	5.25	217	3.53
Acyclovir	0.25	-2.81	-0.39	18.55	187	5.51
Chlorothiazide	0.19	-3.72	3.54	15.94	166	5.11
Griseofulvin	36.6	-10.2	4.16	11.2	245	4.39
Piroxicam	35.6	-5.22	1.72	9.32	215	4.02
Diazepam	33.4	-3.89	-1.45	5.2	215	4.69
Alprenolol	25.3	-5.89	-1.05	5.42	225	5.87
Metoprolol	23.7	-5.91	-0.57	5.53	223	5.89
Corticosterone	21.2	-8.08	-0.64	10.05	240	5.30
Salicyclic Acid	22	-4.99	2.05	4.31	90	4.98
Warfarin	21.1	-8.6	1.28	6.71	205	4.74
Indomethacin	20.4	-9.37	1.72	7.45	247	3.93
Estradiol	16.9	-5.47	-2.53	4.27	193	5.78
Dexamethasone	12.2	-9.39	0.83	5.34	292	5.07
Acetylsalicyclic Acid	9.09	-6.27	3.38	11.1	115	5.39
Zidovudine	6.93	-4.62	4.71	8.79	218	5.28
Nadolol	3.88	-5.45	-1.09	4.9	238	5.82
Sucrose	1.71	-7.09	2.86	11.39	216	8.23
Atenolol	0.53	-5.88	0.64	3.44	247	5.80
Terbutaline	0.47	-5.37	0.31	3.92	187	5.86
Ganciclovir	0.38	-2.85	-0.56	23.02	134	5.47

Table 1(a). P_{app}(BA) for Caco-2 cells [6] for 17 drugs: eq 4

	P(BA) 10^-6 cm/s	$\Delta G_{desolv,CDS}$ kcal/mol	$\Delta G_{lipo,CDS}$ octanol kcal/mol	Dipole Moment D	Molec Volume cm^3/mol	HOMO-LUMO gap eV

Caffeine	27.7	-5.29	0.74	5.7	126	5.04
Progesterone	20.3	7.51	-1.48	7.61	280	5.23
Clonidine	27.1	-0.44	-3.69	2.97	151	5.11
Propranolol	33.2	-4.64	-1.75	4.14	206	4.74
Hydrocortisone	15.9	-8.54	-0.07	12.1	276	5.30
Scopolamine	14.2	-4.21	-0.73	1.99	198	5.50
Bremazocine	19.1	-5.96	-2.04	1.62	284	5.43
Urea	7.91	-3.48	2.46	6.13	54	8.81
Methyl scopolamine	1.78	-7.71	0.15	15.88	248	6.24
Hydrochlorothiazide	1.46	-2.64	3.15	13.5	167	4.92
Acebutolol	10.7	-8	0.69	7.11	282	4.30
Ranitidine	3.49	-5.04	0.26	15.49	241	4.05
Chlorothiazide	2.64	-3.72	3.54	15.94	166	5.11
Testosterone	39.1	-6.27	-1.9	4.98	212	5.29
Telmisartan	42.5	-7.91	-3.26	3.2	335	4.10
Cimetidine	1.67	-4.6	-3.18	4.05	184	6.26
Pirenzepine	2.12	2.28	-1.45	8.09	250	4.42

Table 2. P_{app}(AB) and intrinsic P_{app}(AB) for Caco-2 cells [24] for 58 drugs: eqs 5(a), 5(b) and 5(d)

	P(AB) 10^-6 cm/s	P (AB) Intrinsic 10^-6 cm/s	$\Delta G_{desolv,CDS}$ kcal/mol	$\Delta G_{lipo,CDS}$ octanol kcal/mol	Dipole Moment D	Molec Volume cm^3/mol	HOMO-LUMO gap eV
Acetaminophen (2.0 efflux)	30	58	-5.25	1.76	5.74	111	5.51
Acyclovir (0.88 passive)	0.19	0.16	-2.81	-0.39	18.55	187	5.51
Amiloride (0.42)	1.5	0.64	-2.33	0.14	10.35	148	4.11
Amitryptyline (1.0 passive)	12	13	-3.41	-4.12	1.73	212	5.27
Antipyrine (1.7)	36	60	-5.33	0.27	8.38	147	5.07
Atenolol (0.83 efflux)	0.33	0.28	-5.88	0.64	3.44	247	5.80
Atorvastin (2.0 efflux)	13	25	-13.73	0.29	6.52	394	4.75
Atropine (0.93 passive)	4.3	4	-3.99	-2.27	3.78	251	5.54
Betaxolol (1.6)	12	19	-6.03	-2.40	4.07	214	5.83
Bumetanide (1.0)	1.6	1.7	-8.79	2.88	9.39	203	4.34
Buspirone (1.2 passive)	11	13	-3.52	-4.89	4.78	300	4.75
Bisoprolol (1.5)	6.8	10	-7.11	-1.39	4.6	293	5.87
Caffeine (1.5 passive)	59	90	-5.29	0.74	5.7	126	5.04
Chloramphenicol (1.1)	11	12	-8.63	2.58	8.31	153	4.02
Chlorothiazide (0.91 passive)	0.39	0.35	-3.72	3.56	15.94	166	5.11
Cimetidine (1.1 passive)	0.6	0.68	-4.6	-2.89	4.05	184	6.26
Clozapine (1.0 efflux)	15	15	-1.17	-4.48	7.4	231	4.52

Delavirdine (3.5 efflux)	19	67	-6.4	0.01	6.9	324	3.71
Desipramine (1.7)	14	24	-3.74	-3.58	2.35	209	5.05
Digoxin (2.6 efflux)	2.1	5.5	-15.31	-0.31	10.42	478	5.57
Diltiazem (1.0 efflux)	8.9	8.9	-7.53	0.45	3.99	280	4.78
Domperidone (1.9 efflux)	6.7	13	-5.25	-3.64	2.83	299	5.25
Erythromycin (2.3 efflux)	0.21	0.47	-14.83	0.10	8.68	683	4.95
Fluvastatin (3..4 efflux)	26	88	-10.41	0.13	12.2	280	4.40
Furosemide (12 efflux)	0.05	0.58	-6.77	4.41	8.31	196	4.26
Glibenclamide (1.7)	46	76	-9.22	0.04	9.64	331	5.31
Hydrochlorothiazide (0.91)	0.66	0.6	-2.64	3.21	13.5	167	4.92
Imatinib (1.7 efflux)	10	17	-2.4	-4.33	6	404	3.47
Imipramine (1.0)	22	23	-3.32	-3.98	2.21	232	4.91
Indomethacin (1.1)	97	105	-9.37	1.72	7.45	247	3.93
Inogatran (1.2)	0.09	0.11	-5.66	-2.57	5.7	333	5.30
Ipriflavone (1.1)	59	63	-7.66	0.52	5.39	208	4.49
Irbesartan (1.3)	18	23	-4.78	-1.65	6.21	309	4.86
Ketoprofen (1.1 passive)	85	94	-7.27	1.17	8.26	197	4.82
Lorcainide (1.1)	17	19	-5.03	-4.17	3.02	322	4.89
Melagatran (1.2)	0.08	0.09	-7.26	0.42	6.21	305	5.15
Methotrexate (0.32 efflux)	1.1	0.34	-5.21	1.81	16.14	288	3.33
Metoprolol (1.1 passive)	12	12	-5.91	-0.57	5.53	223	5.89
Midazolam (1.1)	29	31	-7.28	1.14	8.15	182	4.81
Pindolol (0.90)	7.9	7.1	-4.67	-0.78	4.17	199	5.22
Pirenzepine (0.58)	0.26	0.15	-1.44	-1.61	8.39	255	4.50
Piroxicam (1.4)	69	94	-5.3	1.84	9.81	205	4.02
Pravastatin (0.82 efflux)	0.72	0.59	-11.04	1.39	9.48	343	5.21
Prednisolone (1.0 efflux)	21	22	-8.59	0.64	12.72	258	4.96
Propranolol (0.94 passive)	16	15	-4.64	-1.39	4.14	206	4.74
Raloxifene (1.9 efflux)	6.1	11	-7.07	-2.72	4.67	355	3.62
Risperidone (1.2 passive)	11	13	-4.23	-2.77	4.31	314	4.46
Rosuvastatin (2.3 efflux)	0.56	1.3	-11.17	1.66	7.49	383	4.95
Ranitidine (0.58 efflux)	0.55	0.32	-5.04	0.26	15.49	241	4.05
Saquinavir (2.9 efflux)	2	5.7	-11.96	-1.56	10.08	501	3.89
Sildefil Ion (1.2)	39	48	-8.54	0.51	32.63	337	4.17
Sulpirid (0.44)	0.4	0.18	-5.86	1.97	0.79	297	4.46
Talinolol (1.6 efflux)	0.44	0.71	-7.06	-2.30	6.83	336	5.28
Terfenadine (1.4 efflux)	5.3	7.2	-8	-4.96	3.48	360	5.43
Theophylline (1.2)	40	49	-4.82	0.99	5.4	127	5.11
Umbelliferon (1.5 efflux)	34	51	-5.19	2.24	6.28	135	4.33
Verapamil (1.2 efflux)	11	13	-12.13	2.82	10.05	367	5.61
Zolmitriptan (0.27 efflux)	0.95	0.25	-4.24	0.03	10	238	5.10

Footnote: Drugs which are known to be passively transported or actively effluxed are shown with attached parentheses with their efflux ratios (AB Intrinsic P_{app}/AB P_{app}) as per ref [24]. Drugs labeled 'efflux' were used in deriving eq 5(d).

Table 3. "Presumed" passive permeability P(AB) for Caco-2 cells [23] of 19 drugs: eq 6

	P(AB) 10^-6 cm/s	$\Delta G_{desolv,CDS}$ kcal/mol	$\Delta G_{lipo,CDS}$ octanol kcal/mol	Dipole Moment D	Molec Volume cm^3/mol	HOMO-LUMO gap eV
Reserpine	3.5	-13.7	3.86	5.02	440	3.59
Atenolol	3.41	-5.88	0.64	3.41	247	5.80
Sulfadiazine	9.76	-3.35	0.62	11.55	147	4.50
Terbutaline	15.61	-5.37	0.31	3.42	162	5.86
Ketoconazole	9.61	-6.36	-2.61	6.88	381	4.31
Omeprazole	12.58	-5.46	1.20	10.06	270	4.76
Ethionamide	23.75	-2.32	-1.15	5.77	110	4.07
Bupropion	16.64	-5.04	-1.35	2.39	200	4.08
Felodipine	4.34	-10.21	1.35	2.81	290	4.09
Propanolol	10.58	-4.64	-1.75	4.14	206	4.74
Chloramphenicol	8.17	-8.63	2.58	8.31	153	4.02
Metoprolol	12.05	-5.91	-0.57	5.53	223	5.89
Verapamil	10.05	-12.13	2.82	10.05	367	5.61
Lamotrigine	18.49	-1.48	-1.76	6.04	167	4.73
Warfarin Sodium	15.31	-8.64	2.62	4.53	181	4.23
Naproxen	15.01	-7.11	1.62	4.46	166	4.46
Nifedipine	10.69	-12.29	5.79	5.23	265	2.64
Ketoprofen	19.19	-7.27	1.17	8.26	197	4.82
Carbamazepine	20.85	-6.29	-0.46	6.08	149	4.55

Table 4. Passive permeability log P(AB) of Caco-2 cells [12] for 36 drugs: eq 7

	Log P(AB)	$\Delta G_{desolv,CDS}$ kcal/mol	$\Delta G_{lipo,CDS}$ octanol kcal/mol	Dipole Moment D	Molec Volume cm^3/mol	HOMO-LUMO gap eV
Coumarin	-4.11	-4.62	1.31	7.52	108	4.61
Theophylline	-4.35	-4.82	0.99	5.4	127	5.11
Mannitol	-5.58	-4.76	2.27	3.38	137	8.99
Epinephrine	-6.02	-3.24	0.77	3.98	132	5.84
Guanoxan	-4.71	-2.35	-0.93	5.45	149	5.60
Terbutaline	-6.42	-5.37	0.31	3.42	162	5.86
Guanabenz	-4.14	-3.77	-1.56	6.12	159	4.34
Lidocaine	-4.21	-5.77	-0.74	5.55	181	5.21
Alprenolol	-4.39	-5.89	-1.05	5.42	225	5.87
Propranolol	-4.38	-4.64	-1.75	4.14	206	4.74
Tiacrilast	-4.9	-6.67	2.27	11	192	3.63

Practolol	-5.86	-6.14	0.66	5.72	228	5.50
Atenolol	-6.63	-5.88	0.64	3.41	247	5.80
Metoprolol	-4.57	-5.91	-0.57	5.53	223	5.89
Imipramine	-4.26	-3.32	-3.98	2.21	232	4.91
Testosterone	-4.23	-6.27	-1.90	4.98	212	5.29
Olsalazine	-6.96	-7.82	5.14	0.52	191	3.47
Warfarin	-4.27	-8.6	1.28	6.71	205	4.74
Furosemide	-6.09	-6.77	4.41	8.31	196	4.26
Sulpiride	-6.16	-5.86	1.97	0.79	297	4.46
Corticosterone	-4.26	-8.08	-0.64	10.05	240	5.30
Nitrendipine	-4.77	-12.87	5.53	5.5	219	2.72
Hydrocortisone	-4.67	-8.54	-0.07	12.1	276	5.30
Fleroxacin	-4.81	-5.67	0.93	14.03	205	3.95
Felodipine	-4.64	-10.21	1.35	2.81	290	4.09
Dexamethasone	-4.9	-9.39	0.83	5.34	292	5.07
Sulphasalazine	-6.89	-6.85	3.76	5.25	217	3.53
Diltiazem	-4.31	-7.53	0.45	3.99	280	4.78
Verapamil	-4.58	-12.13	2.82	10.05	367	5.61
Mibefradil	-4.87	-9.26	-1.66	4.76	322	5.27
Bosentan	-5.98	-8.83	1.36	8.98	384	4.01
Proscillaridin	-6.2	-11.33	0.45	12.3	335	4.53
Ceftriaxone	-6.88	-10.72	6.6	18.52	341	3.58
Remikiren	-6.13	-10.89	-2.17	8.58	424	5.68
Saquinavir	-6.26	-11.96	-1.56	10.08	501	3.89
Bosentan Alternate Configuration	-5.98	-8.42	1.05	6.97	344	4.08